Metrol. Meas. Syst., Vol. 26 (2019) No. 4, pp. 697–711
DOI: 10.24425/mms.2019.130567

METROLOGY AND MEASUREMENT SYSTEMS
Index 330930, ISSN 0860-8229
www.metrology.pg.gda.pl

ADAPTIVE FILTERING-BASED CURRENT RECONSTRUCTION IN NON-CONTACT MAGNETIC SENSOR ARRAY MEASUREMENT SYSTEM

Yafeng Chen, Qi Huang

University of Electronic Science and Technology of China, The Sichuan Provincial Key Lab of Power System Wide-Area Measurement and Control, Chengdu 611731, Sichuan, China (✉ *hwong@uestc.edu.cn*, +86 028 6183 1087, *yafengchen2015@163.com*)

Abstract

The non-contact current measurement method with magnetic sensors has become a subject of research. Unfortunately, magnetic sensors fail to distinguish the interested magnetic field from nearby interference and suffer from gauss white noise due to the intrinsic noise of the sensor and external disturbance. In this paper, a novel adaptive filtering-based current reconstruction method with a magnetic sensor array is proposed. Interference-rejection methods based on two classic algorithms, the least-mean-square (LMS) and recursive-least-square (RLS) algorithms, are compared when used in the parallel structure and regular triangle structure of three-phase system. Consequently, the measurement range of RLS-based algorithm is wider than that of LMS-based algorithm. The results of carried out simulations and experiments show that RLS-based algorithms can measure currents with an error of around 1%. Additionally, the RLS-based algorithm can filter the gauss white noise whose magnitude is within 10% of the linear magnetic field range of the sensor.

Keywords: current measurement, adaptive filtering, sensor array, gauss white noise.

1. Introduction

Advanced technologies to provide accurate parameter information such as active power, reactive power and measured current are of great significance for the development of a smart grid [1–3]. Especially, a high-accuracy current information is the key to the safety and reliability of a modern power system. Conventional current transformers use a closed magnetic core to transform the magnetic field signal into the electric current signal. However, due to the magnetic core, the transformer encounters the problem of saturation, which can cause false current waveforms with distortion [4]. Besides, the closed structure of the transformer is inconvenient for installation and disassembly [5]. Due to the shortcomings of the traditional current transformers, novel current measurement devices have attracted more and more attention of researchers [6]. A non-contact current measurement method with magnetic sensors proves to be an effective approach that can overcome the two aforementioned disadvantages. These devices are free from the saturation

problem of the magnetic core and are physically flexible. Nevertheless, using a magnetic sensor to measure current needs to deal with one problem: the superposition of the magnetic field and magnetic interference from external current sources. Conventional current transformers block the nearby magnetic interference with the magnetic core. However, the magnetic sensors, due to their high sensitivity, fail to distinguish the interfering magnetic field from the magnetic field generated by the current under measurement [7, 8]. Therefore, some approaches have been proposed to alleviate the effect caused by the magnetic interference.

One of the approaches is the sum-average algorithm [9–12], which utilizes the averaging of the magnetic field detected by the sensors to estimate the current under measurement. However, when the nearby magnetic field is much stronger than the magnetic field generated by the current under measurement, the estimated error is large [13, 14]. Additionally, the interference is regarded as a virtual current generated by one nearby conductor [15, 16]. For the three-phase current system, when measuring a one-phase current, the other two one-phase currents function as interfering sources. Another problem for a magnetic sensor is the noise from the intrinsic and background interference. This kind of noise is random and is regarded as gauss white noise [17], which can have an influence on the accuracy of the magnetic field measurement. Nevertheless, the sum-average algorithm cannot remove the gauss white noise. Therefore, there is an urgent need to develop novel methods of reducing the influence of magnetic interference in current measurement in the three-phase current system.

Adaptive filtering algorithms have been widely used for eliminating gauss white noise in processing communication signals [18]. In recent years, some works have dealt with applying the adaptive filtering algorithms to power systems [19–23]. In [19], the authors proposed a Lorentzian norm-based adaptive filter to control Voltage Source Converter in a wind-driven distributed generation system. In [20], a prediction-error covariance estimator for adaptive Kalman Filtering was proposed and validated in the case of power system state estimation. In [21], an algorithm based on *recursive-least-squares* (RLS) and *iterated extended Kalman filter* (IEKF) techniques was designed to estimate the real-time harmonics in a power system. In [22], the authors used a robust RLS approach to assess conservation voltage reduction in a power distribution system. In [23], a robust RLS algorithm was demonstrated for online identification of power system modes. In particular, the authors in [24] designed an optimal steady-state filtering and a sub-optimal steady-state filtering based on Kalman Filtering for non-contact current measurement. The application of optimal filtering was limited because it relied on the information of characteristics of the system status, which was unknown in a real scenario. Sub-optimal filtering was proposed to compensate this shortcoming. However, only currents up to a few amperes were tested and the error reached up to 5%.

Inspired by these works, in this paper, an adaptive filtering algorithm is applied to measure one-phase current in the three-phase current system. Since the *least-mean-square* (LMS) [25, 26] and RLS [27–29] algorithms are two classical adaptive filtering algorithms with the advantages of computational efficiency, simple code and robustness in relation to disturbances [18, 30], interference-rejection algorithms based on the LMS and RLS algorithms are proposed and compared to be used for non-contact current measurement with a magnetic sensor array.

The goals of this paper include:

– to reduce the influence of other two one-phase currents when one one-phase current is under measurement;
– to demonstrate the effectiveness of the adaptive filtering-based algorithms when applied to two structures of the three-phase current system in medium-voltage and low-voltage power networks;

Metrol. Meas. Syst., Vol. 26 (2019), No. 4, pp. 697–711
DOI: 10.24425/mms.2019.130567

– to examine how the algorithms are affected by such factors as the parameters in adaptive filtering, number of sensors, sensor position and conductor displacement;
– to prove the capability of the algorithms to filter out the gauss white noise caused by the intrinsic noise of sensors and external disturbances.

The rest of the paper is organized as follows. In Section 2, the mathematic principles of LMS-based and RLS-based algorithms are analysed. In Section 3, there are described simulations examining the influence of the number of sensors, learning rate and forgetting factor, sensor position, conductor displacement and current magnitude. In Section 4, there are presented FEA simulations and laboratory experiments analysing the RLS-based algorithm applied to current measurement. Conclusions are presented in Section 5.

2. Mathematical background

The three-phase alternating current system usually has two types of structure, as shown in Fig. 1. In this paper, a sensor array consisting of four uniformly placed magnetic sensors (S_1, S_2, S_3 and S_4) is proposed to measure one-phase current. The case when I_1 is the target current is used as an instance to illustrate the mathematical principle of the algorithms. As shown in Fig. 1, the distance between two conductors is d, which is within a range of 0.5 m. The distance between the target conductor and sensor is r. B_{11}, B_{12}, and B_{13} are magnetic fields generated by I_1, I_2 and I_3, respectively. Magnetic sensors can detect the magnetic field along the sensitive direction of sensors. For example, for S_1, the direction is along the direction of B_{11}. Due to the superposition of the magnetic fields, the detected magnetic field (B_1 to B_4) by S_1 to S_4 can be determined theoretically based on Biot-Savart Law as:

$$\begin{cases} B_1 = \dfrac{\mu I_1}{2\pi r} + \dfrac{\mu I_2 r}{2\pi(d^2+r^2)} + \dfrac{\mu I_3 r}{2\pi(d^2+r^2)} \\ B_2 = \dfrac{\mu I_1}{2\pi r} - \dfrac{\mu I_2}{2\pi(d-r)} + \dfrac{\mu I_3}{2\pi(d+r)} \\ B_3 = \dfrac{\mu I_1}{2\pi r} + \dfrac{\mu I_2 r}{2\pi(d^2+r^2)} + \dfrac{\mu I_3 r}{2\pi(d^2+r^2)} \\ B_4 = \dfrac{\mu I_1}{2\pi r} + \dfrac{\mu I_2}{2\pi(d+r)} - \dfrac{\mu I_3}{2\pi(d-r)} \end{cases}, \tag{1}$$

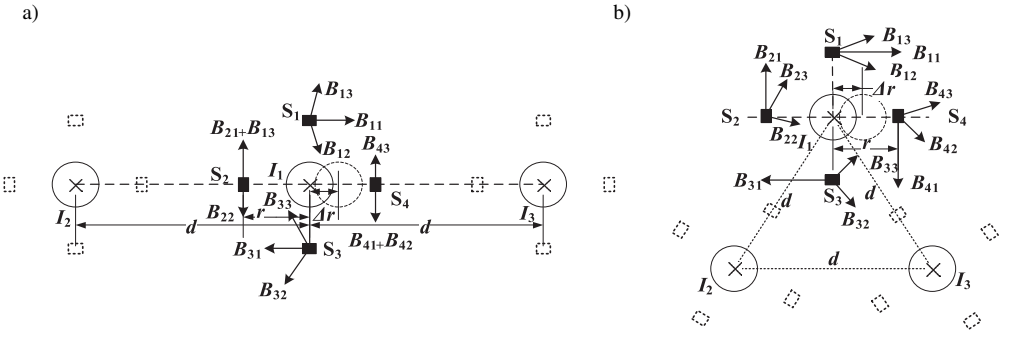

Fig. 1. Structures of the three-phase alternating current system: a) parallel; b) regular triangle.

where μ is the permeability of free space. In this case, I_2 and I_3 serve as the interfering currents. When measuring the other two one-phase currents, the placements of the sensors are respectively depicted by dotted lines in Fig. 1.

In this paper, interference-rejection algorithms based on the LMS and RLS are proposed and examined.

2.1. LMS-based algorithm

The main idea of LMS-based adaptive filtering algorithm is to minimize the squared error between the filtered output signal and the reference signal (also called the desired signal), which is obtained by updating the filtered weights of w, the initial value of which can be set to 0. That is, $w = [0, 0, \ldots, 0]_{1\times M}$, where M is the input dimensionality. In this paper, the input signals are the magnetic fields detected by the sensors. The final filtered output signal is the current magnitude. With the interference from other two one-phase currents, information on the target current is unknown. Some works [9–12]have demonstrated that the sum-averaging algorithm is an acceptable method to eliminate the interfering magnetic field from other current sources. Therefore, the desired signal is the current of I_{ave} determined by the average of the detected magnetic fields according to Biot-Savart Law. Assuming the number of sensors is P, there are P filtered output signals, among which the filtered signal with the smallest error between the filtered signal and the desired signal is taken as the final output. In this paper, P is equal to 4. After the filtering, there will be P current signals. The final current I_{final} is determined by choosing a signal I_q ($q \in \{1, 2, \ldots, P\}$) whose magnitude at the peak value is closest to the desired signal. Therefore, the whole process can be expressed as shown in Table 1, where B_i is the magnetic field detected by sensor S_i, $\widetilde{I}_i$ is the processed output of magnetic field with filtered weights, u is a parameter called learning rate in LMS algorithm. The magnetic field detected in a period of time is selected as the input of LMS-based algorithm. This period of time is divided into N sampling points and n can be any one of the sampling points, which should be less than or equal to N. Then, the error between the filtered current signal at the peak value and the real current at the peak value can be determined.

Table 1. The LMS filtering algorithm-based current reconstruction.

Training Sample:	Input: B_i, $i = 1, 2, \ldots, P$ Desired Signal: $I_{\text{ave}} = \frac{1}{P}\left(\frac{2\pi r B_1}{\mu_0} + \cdots + \frac{2\pi r B_P}{\mu_0}\right)$
User-selected Parameter:	u
Initialization:	$w(n) = [w_1(n), w_2(n), \ldots, w_M(n)] = [0, 0, \ldots, 0]_{1\times M},\ 0 \le n \le N$
Computation:	$\widetilde{I}_i(n) = \sum_{k=1}^{M} w_k(n) B_i(n - M + k - 1)$ $w(n+1) = w(n) + 2ueB_i(n)$ $e(n) = I_{\text{ave}}(n) - \widetilde{I}_i(n)$
Finalization:	if $Max[I_q] - Max[I_{\text{ave}}] \le Max[I_i] - Max[I_{\text{ave}}]$ then $I_{\text{final}} = I_q$

Metrol. Meas. Syst., Vol. 26 (2019), No. 4, pp. 697–711
DOI: 10.24425/mms.2019.130567

2.2. RLS-based algorithm

The main idea of RLS algorithm is similar to that of LMS algorithm. Nevertheless, differently from LMS algorithm which updates the filtered weights after the filtered output, the error signal in RLS algorithm is obtained with the difference between the desired signal and the newest updated filtered weights. In the RLS-based algorithm, the average of the magnetic fields detected according to Biot-Savart Law is taken as the desired signal. Similarly to the LMS-based algorithm, the final current I_{final} is determined by choosing a signal I_q ($q \in \{1, 2, \ldots, P\}$), the error between which and the desired signal is the smallest. The whole process is presented in Table 2, where λ ($0 \ll \lambda \leq 1$) is called a forgetting factor, E is a unit matrix of M-order, K is a gain vector.

Table 2. The RLS filtering algorithm-based current reconstruction.

Training Sample:	Input: B_i, $i = 1, 2, \ldots, P$ Desired Signal: $I_{\text{ave}} = \frac{1}{P}\left(\frac{2\pi r B_1}{\mu_0} + \cdots + \frac{2\pi r B_P}{\mu_0}\right)$
User-selected Parameter:	λ
Initialization:	$w(n) = [w_1(n), w_2(n), \ldots, w_M(n)] = [0, 0, \ldots, 0]_{1\times M}$, $S_D = E, 0 \leq n \leq N$
Computation:	$\widetilde{I}_i = \sum_{k=1}^{M} w_k(n) B_i(n+k-1)$ $K = \frac{S_D B_i^T}{\lambda + B_i S_D B_i^T}$ $S_D = \frac{1}{\lambda}(S_D - K B_i S_D)$ $w(n+1) = w(n) + +K(I_{\text{ave}} - \widetilde{I}_i)$
Finalization:	if $Max[I_q] - Max[I_{\text{ave}}] \leq Max[I_i] - Max[I_{\text{ave}}]$ then $I_{\text{final}} = I_q$

3. Assessment of algorithm parameters

Numerical simulations were carried out to analyse the effects caused by the number of sensors, the position of the sensor, the learning rate of LMS-based algorithm and the forgetting factor of RLS-based algorithm. The amplitude *relative error* (RE) between the filtered result at the peak value and the real current signal at the peak value was used to examine these effects. For the parameters of the numerical model, the distance d between two conductors was 0.3 m. The distance between the sensor and conductor was 0.015 m. The two algorithms were finally tested in the three-phase current measurement in two different structures. $i_1(t)$ was the target current. $i_1(t)$ was $I_m \sin(100\pi t)$, $i_2(t)$ was $I_m \sin(100\pi t - 2\pi/3)$ and $i_3(t)$ was $I_m \sin(100\pi t + 2\pi/3)$ while I_m changed from 50 A to 600 A. So, the amplitude relative error can be determined by

$$RE = \left|\frac{I_{mf} - I_m}{I_m}\right| \times 100\%, \tag{2}$$

where I_{mf} is the peak value of the filtered current signal.

3.1. Learning rate and forgetting factor

The impact of the learning rate and the forgetting factor on the filtered output signal is first analysed for the parallel structure. I_m is set to 600 A. For the LMS-based algorithm, the learning rate u controls the convergence rate of the Mean Squared Error. Therefore, the value of learning rate has an effect on the convergence performance of the LMS algorithm and the filtering results. At the beginning period of 4 ms, the filtered output signal is zero for the initial filtered weights are zero. As shown in Fig. 2a, the estimated results of the current vary in relation to the change of the learning rate. When the learning rate increases, the amplitude relative error becomes smaller. When the learning rate is 1000, the error is 7%. However, there is a time delay between the reference value of the target current and the estimated result, about 1.5 ms. Nevertheless, when the learning rate is 5000, the error is 2%. However, the error is not always negatively correlated with the learning rate. For example, when the learning rate is 8000, the error becomes as large as 26%. Further performance of the algorithm is assessed with the changing frequency of the current. The results are presented in Table 3. For the LMS-based algorithm, it can be noted that the amplitude relative error is negatively correlated with frequency.

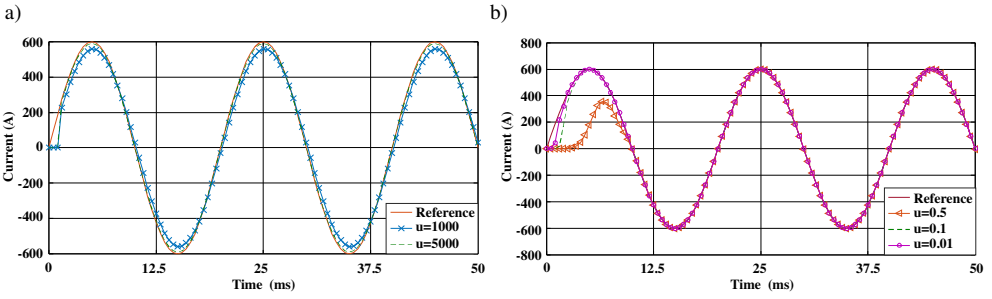

Fig. 2. Filtered current vs. time a) with different learning rate values; b) with different forgetting factor values.

Table 3. Current amplitude relative error (%) vs. frequency.

Frequency (Hz)	50	60	70	80	90
u = 1000	7	7	5	4	2
u = 5000	1	0.4	5×10^{-2}	2×10^{-3}	6×10^{-4}
λ = 0.1	9×10^{-3}	0.7	3.00	7	14
λ = 0.01	6×10^{-4}	6×10^{-4}	6×10^{-4}	6×10^{-4}	6×10^{-4}

In the RLS algorithm, the forgetting factor λ suggests the increasingly negligible effect of the distance information on the coefficient updating. It can be seen in Fig. 2b that the filtered output signal takes less time to be close to the reference of I_1 when the forgetting factor is smaller. Additionally, when the forgetting factor is 0.1, the error is 9×10^{-3}% at the first peak value of the current. When the forgetting factor is 0.01, the error is 6×10^{-4}%. Besides, the error becomes smaller as the sampling time becomes longer. For instance, for the forgetting factor of 0.1, the error is 9×10^{-3}% at the time of 5 ms. Nevertheless, the error becomes 6×10^{-4}% at the time of 15ms. This phenomenon does not exist in the LMS-based algorithm. However, when the factor is too small, such as 0.0001, or when the factor is large, such as 1, the algorithm fails to filter the signal.

Metrol. Meas. Syst., Vol. 26 (2019), No. 4, pp. 697–711
DOI: 10.24425/mms.2019.130567

For the following parts, the error discussed is at the first peak value of the current.

Then, the relationship between the error and the frequency of the current is examined. The results are shown in Table 3. It can be seen that when λ is 0.1, in contrast to the consequence of LMS-based algorithm, the error is positively correlated with the frequency of the current. Nevertheless, when λ is 0.01, the error remains at 6×10^{-4}%, which suggests that the filtered result is much closer to the desired signal.

Since the current signal in a power system contains higher harmonics, the effects caused by the poly-harmonics are analysed. Assuming the target current $I_1(t)$ is $600\sin(100\pi t) + N_m \sin(1000\pi t)$, when N_m is 10, 20 and 30, respectively, the results obtained with the LMS-based and RLS-based algorithms are depicted in Fig. 3. It can be seen that the LMS-based algorithm gives better results when N_m is 10. Nevertheless, when the amplitude of harmonics becomes larger, the algorithms fail to remove the harmonics.

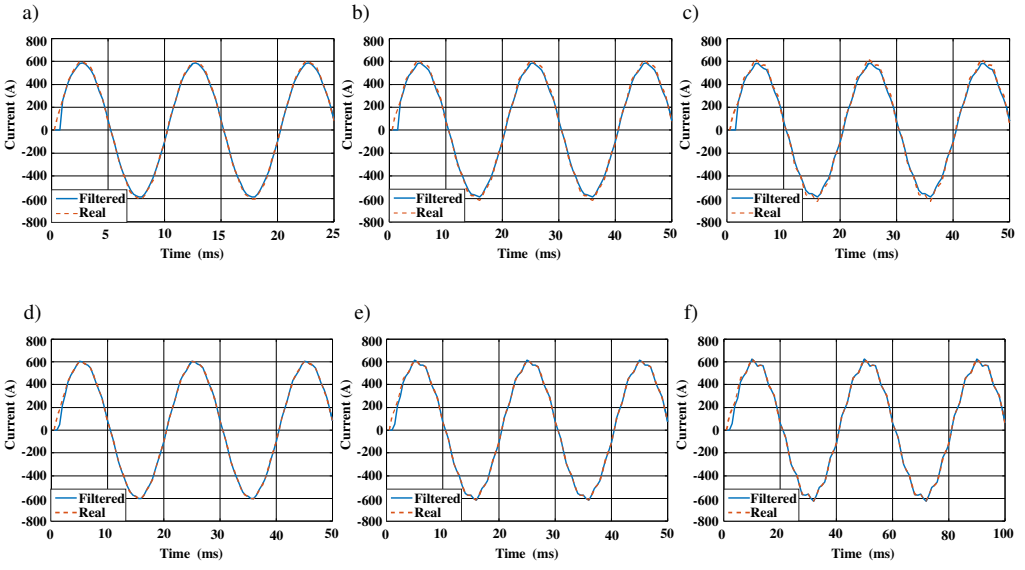

Fig. 3. Filtered current vs. different amplitude of harmonics. a) $N_m = 10$ by LMS-based algorithm; b) $N_m = 20$ by LMS-based algorithm; c) $N_m = 30$ by LMS-based algorithm; d) $N_m = 10$ by RLS-based algorithm; e) $N_m = 20$ by RLS-based algorithm; f) $N_m = 30$ by RLS-based algorithm.

3.2. Numbers of sensors

In numerical simulations, effects caused by the number of sensors are examined. I_m changes from 50 A to 600 A. For the LMS-based algorithm, the learning rate is set to 5000. For the RLS-based algorithm, the forgetting factor is set to 0.1. The cases of two, three and four sensors have been tested. The error between the reference current and the estimated magnitude at peak is calculated. Arrangements of sensors are shown in Fig. 4. The results are shown in Fig. 5. For the LMS-based algorithm, the error decreases with more sensors. However, for the current less than 100 A, the error is larger than 6%. For the current up to 600 A, the error can reach up to 9%. Since the updated weight is influenced by the fixed learning rate, the LMS-based algorithm has an effective filtering range. For the RLS-based algorithm, it can be noted that there is a negative correlation between the error and the number of sensors and that the error is negatively correlated

with the current amplitude. Nevertheless, the error becomes larger with an increase of current amplitude when only three sensors are employed in the regular triangle structure, which is not suitable for measurement of large currents. Compared with the results obtained for the parallel structure, this is caused by the structure difference. For instance, when I_m is 600 A, at 5.5 ms, for sensor S_2, the combined magnetic flux density coming from I_2 and I_3 is 0.1682 Tesla. In the parallel structure, the combined magnetic flux density is 0.01 Tesla, much smaller than that in the triangular structure. So, as the magnitude increases, the filtered signal has a larger error when the forgetting factor is fixed. When the RLS-based algorithm is used with four sensors, the maximum error is 1% for the current ranging from 50 A to 600 A. The effective range of RLS-based algorithm is larger than that of LMS-based algorithm. Therefore, compared with the LMS-based algorithm, the RLS-based algorithm with a four-sensor structure is more stable and can achieve a higher accuracy. Additionally, even though more sensors will cause more power consumption, four sensors are employed in the proposed method.

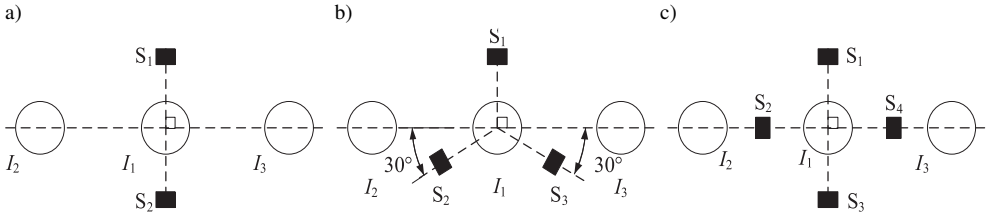

Fig. 4. Arrangements of sensor array a) 2 sensors; b) 3 sensors; c) 4 sensors.

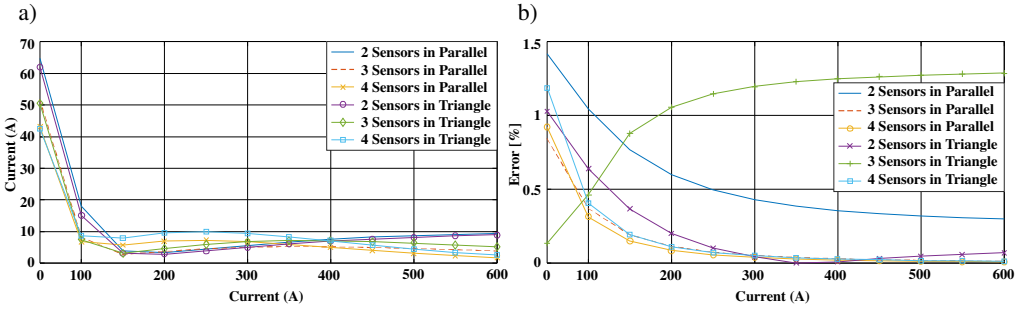

Fig. 5. Error vs. current amplitude with different numbers of sensor a) for the LMS-based algorithm; b) for the RLS-based algorithm.

3.3. Sensor position

Numerical simulations are then performed to analyse the influence of the sensor position in the parallel structure and regular triangle structure, respectively. Four sensors are used and the distances between each sensor and the target conductor are the same. I_m is set to 600 A. For the LMS-based algorithm, the learning rate is set to 5000. For the RLS-based algorithm, the forgetting factor is set to 0.1. The distance between sensor and the conductor changes from 0.015m to 0.025m. The results in Fig. 6 show that the RLS-based algorithm displays a higher accuracy than the LMS-based algorithm. For both algorithms in the triangle structure, the error between the reference magnitude and the estimated current at the peak value of the current increases as the

Metrol. Meas. Syst., Vol. 26 (2019), No. 4, pp. 697–711
DOI: 10.24425/mms.2019.130567

distance between sensor and the conductor increases. However, for both algorithms in the triangle structure, the error is not strictly positively correlated with the distance between sensor and the conductor. In addition, the error variance (error divided by minimum error) for the LMS-based algorithm is 160% in the parallel structure and 263% in the regular triangle structure, while the error variance for the RLS-based algorithm is 130% in the parallel and 250% in regular triangle structure, respectively. The RLS-based algorithm shows better stability compared with the LMS-based algorithm.

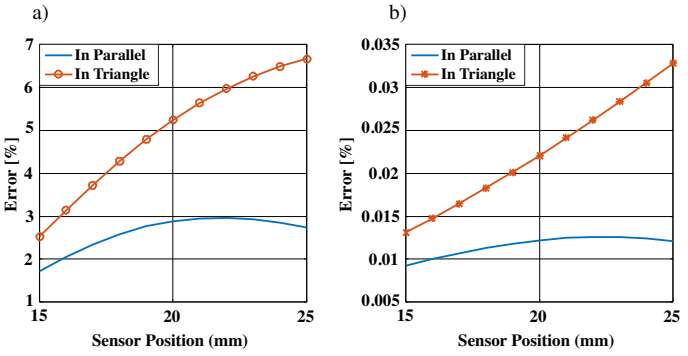

Fig. 6. Error vs. sensor position a) LMS-based algorithm; b) RLS-based algorithm.

3.4. Conductor displacement

Above discussions assume that the conductor is at the sensor array centre. However, a conductor displacement may occur when installing the sensor array. This part examines the influence contributed by the conductor displacement. In this part, a conductor displacement is defined as a single conductor moved relative to other conductors. In the parallel structure, the target conductor moves along the line connecting the centres of the three conductors. In the triangular structure, it moves along the line connecting the centres of the target conductor, S_2 and S_4 (see Fig. 1). Due to the symmetry of the two structures, the situation that the conductor moves to the right side is discussed. For the LMS-based algorithm, the learning rate is set to 5000. For the RLS-based algorithm, the forgetting factor is set to 0.1. I_m is set to 600 A. I_1 is the target current, which moves to the position represented by the dotted line in Fig. 1, with a translation distance of Δr. The estimated errors at the peak value of the current obtained with the LMS-based and RLS-based algorithms are depicted in Fig. 7. It can be seen that the error obtained with the RLS-based algorithm is larger when the conductor displacement exceeds 6 mm. When the conductor displacement is 10 mm, the error reaches up to 25% while it is 14% for the LMS-based algorithm. In the regular triangle structure, the maximum error obtained with the RLS-based algorithm is 25% while for the LMS-based algorithm it is 13%. Nevertheless, the LMS-based algorithm yields a larger error than the RLS-based algorithm when the displacement is within 6 mm. In addition, the error obtained with the LMS algorithm is not strictly correlated with the displacement. When the displacement is 6 mm in the parallel structure, the error obtained with the LMS-based algorithm is minimum, which is 0.4%. For the displacement of 7 mm in the triangular structure, the error of 0.5% is the minimum one. Therefore, considering a small size of the measurement structure, compared with the LMS-based algorithm, the RLS-based algorithm still shows better performance.

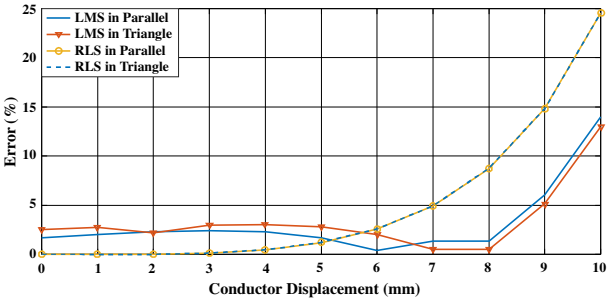

Fig. 7. Error vs. conductor displacement.

4. Validation of RLS-based algorithm

4.1. Normal signal

4.1.1. Laboratory experiments

From the above results, the RLS-based algorithm shows better performance with a smaller error. Laboratory experiments were then carried out to examine the effectiveness of RLS-based algorithm in measurement of three-phase alternating current. The arrangement of experimental equipment is shown in Fig. 8. A 220 V commercial power of 50 Hz supplies three resistive loads. The peak-to-peak value of each phase is presented in Table 4. A current probe, A621 from Tektronix, is employed to measure current as the reference value. Four *Tunnel Magnetoresistance* (TMR) sensors are uniformly placed in a panel, constituting an array. The type of sensor is TMR2104, from dowaytech [31]. The current-carrying conductor with a radius of 5 mm is placed at the centre of the sensor array. The displacement error of sensors is within ±0.01 mm. The displacement of conductor is within 1 mm. At a laboratory temperature of 25°, the used TMR has a linear output when the range of the applied magnetic field is within ±80 Gauss. Therefore, the maximum magnitude of current should be smaller than 600 A. A stable DC power source, LM337t of 3 V, supplies the sensor array circuit. The distance between the conductor and sensor is set to 1.5 cm. All the data are recorded in an oscilloscope, MDO3012 from Tektronix. The resolution bandwidth is 10 kHz. The sample rate is 100 kS/s.

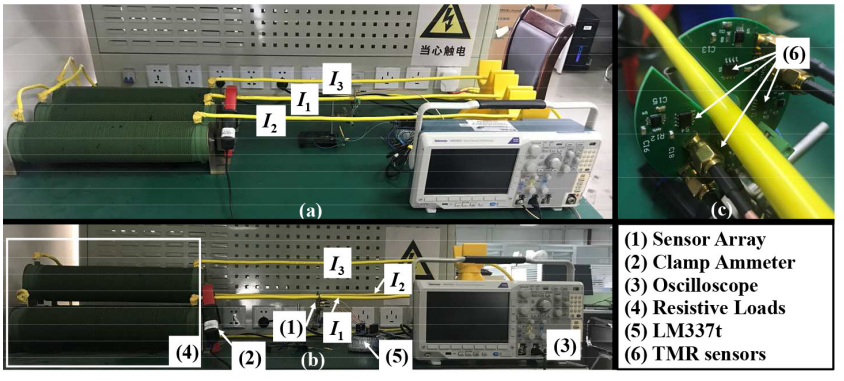

Fig. 8. The arrangement of laboratory experiment a) experiment for the parallel structure; b) experiment for the regular triangle structure; c) arrangement of the sensor array.

Metrol. Meas. Syst., Vol. 26 (2019), No. 4, pp. 697–711
DOI: 10.24425/mms.2019.130567

Since the temperature and the supply voltage influence the sensitivity of the TMR sensor, calibration experiments were first performed to determine the relationship between the current under measurement and the magnetic field generated by it. With data fitting, the sensitivity was determined as 3.085 mV/V/Gauss. Based on the definition of sensor sensitivity from the datasheet, the relationship between the magnetic field and the output voltage of the sensor can be expressed as:

$$Output\ Voltage = 3.085 V_{sp} F_g B, \tag{3}$$

where: V_{sp} is the supply voltage; F_g is the gain factor and B is the detected magnetic flux density. In the experiments, the supply voltage is 3 V and the gain factor of the amplifier INA333 is 2. The laboratory experiments were then performed for each phase current in the parallel and regular triangle structures. The distance between two adjacent conductors in two structures was 0.3 m. The results are presented in Table 4. It can be seen that for the RLS-based interference-rejection algorithm, the error at the peak value of the current is less than 2%. The minimum error is 1 %. Compared with the results of numerical simulations, the error is larger. Due to the complexity of the laboratory experiments, the error is mainly contributed by the displacement of the conductors, sensors, and the magnetic interference from nearby electrical equipment. In addition, errors also come from the current probe and digital oscilloscope.

Table 4. Amplitude relative error values (%) between the filtered and reference currents of each phase.

Phase	Reference Value (A)	Error (%)	
		In parallel	In Triangle
I_1	42.4	1	2
I_2	42.8	2	2
I_3	41.6	2	2

4.1.2. FEA simulations

Due to the limited scope of the experiments, larger currents were tested by the *finite element analysis* (FEA) method in ANSYS Maxwell 16.0 to examine the cases where the RLS-based algorithms were applied to direct current measurement. In accordance with the above discussion, the simulation model was constructed as shown in Fig. 9. The currents flow along the positive z axis in the copper conductor. The simulations were performed when the magnitude of the direct current changed from 50 A to 600 A. The conductors were placed in a vacuum box region, which

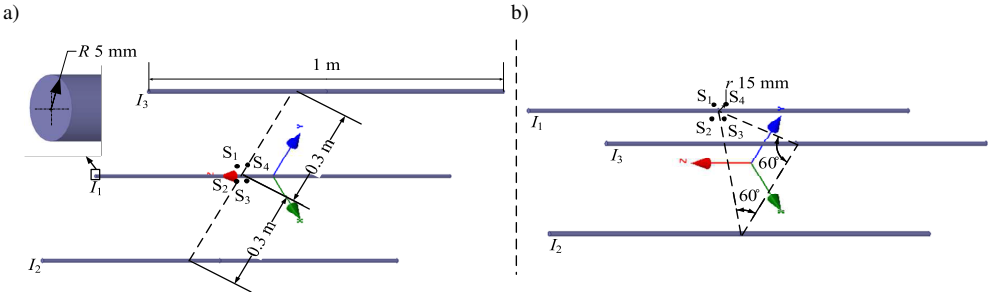

Fig. 9. The simulation model a) in the parallel structure; b) in the regular triangle structure.

was four times larger than the current system. The element length-based refinement was chosen for the mesh operations. The maximum length of elements was set to 100 mm. For the conductors, the maximum length of elements was set to 10 mm. Due to the symmetry of the structure, only I_1 and I_2 are discussed as the target currents in the parallel structure while only I_1 is discussed as the current under measurement in the regular triangle structure. When the current-to-be-measured is 600 A, the algorithm becomes non-convergent. For the RLS-based algorithm, the results are depicted in Fig. 10a. It can be seen that the error is less than 0.8 % in two structures. The error in direct current measurement does not change in relation to the varying of the current magnitude because the magnitude of direct current keeps the same, as a result of which, the error is insensitive to the direct current magnitude.

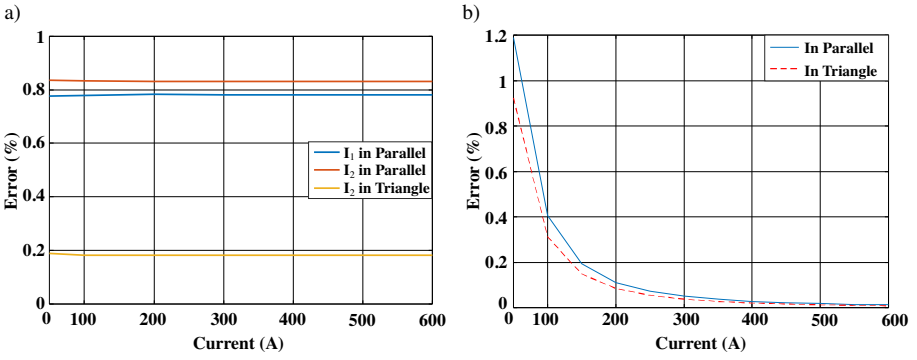

Fig. 10. Error vs. magnitude of current a) direct current; b) alternating current.

The tests were carried out to examine the effectiveness of the two algorithms for alternating currents in a wider range. The model settings were the same as those for direct current simulation. The simulation time was 50 ms with a time step of 0.05 ms. $i_1(t)$ was $I_m \sin(100\pi t)$, $i_2(t)$ was $I_m \sin\left(100\pi t - \frac{2\pi}{3}\right)$ and $i_3(t)$ was $I_m \sin\left(100\pi t + \frac{2\pi}{3}\right)$ while I_m changed from 50 A to 600 A. Since the first peak of $i_2(t)$ occurred when t was 6.7 ms while the initial filtered weights were zero at the beginning period of 4 ms, the error at the second peak value of the $i_2(t)$ is discussed. For $i_2(t)$, the estimated error obtained with the RLS-based algorithm remains 6×10^{-4}% in the parallel and regular triangle structures. For $i_3(t)$, the error remains 3×10^{-4}% in both parallel and triangle structures. Other estimated results are shown in Fig. 10b. When I_m is set to 600A, the specific errors between the reference magnitude of each phase current and the filtered result at the peak value of the current are presented in Table 5. Still, it can be seen that the RLS-based algorithm exhibits high accuracy. It should be noticed that the magnetic field generated in the FEA simulations is not exactly the same as the theoretical value obtained by Biot–Savart Law. Due to the symmetry of parallel structure, the errors for both I_2 and I_3 currents should be the

Table 5. Error (%) obtained with the adaptive filtering algorithm in different structures.

Structure	In parallel	In Triangle
I_1	0.01	0.01
I_2	6×10^{-4}	6×10^{-4}
I_3	3×10^{-4}	3×10^{-4}

Metrol. Meas. Syst., Vol. 26 (2019), No. 4, pp. 697–711
DOI: 10.24425/mms.2019.130567

same. Similarly, in the triangle structure, the errors for all currents I_1, I_2 and I_3 should be the same. However, the results are not the same due to the difference between the simulated magnetic field and the theoretical one.

4.2. Noisy signal

In real scenarios, the magnetic field signal under measurement will be contaminated by factors like the intrinsic noise of magnetic sensors, noise from the geomagnetic field and noise from nearby electrical equipment. Sum-average algorithms cannot remove the disturbance of the white gauss noise. Due to the filtering function of adaptive filtering algorithms, one advantage of the RLS-based interference-rejection algorithm is the ability to remove these noises. Since these noises are uncorrelated, the random white gauss noise of a standard normal distribution is added to the signal detected by the sensors [17]. When the peak current value is 600 A, the magnetic field is 80 Gauss. So, gauss white noises with amplitudes of 5%, 10% and 15% of 80 Gauss were tested. The results estimated by the RLS-based algorithm in two structures are shown in Fig. 11. It can be seen that after the second period, the current signal becomes much smoother with the RLS-based filtering algorithm when the gauss white noise is within 10% of the strength of the detected magnetic field. The standard deviation of the difference between the filtered signal and the real current signal is calculated based on the data from the period between 20 ms and 50 ms. In the parallel structure, the standard deviation is 11 A. In the triangular structure, the standard deviation is 24 A. This is larger than the standard deviation in the parallel structure due to the stronger effect caused by the noise in the triangular structure.

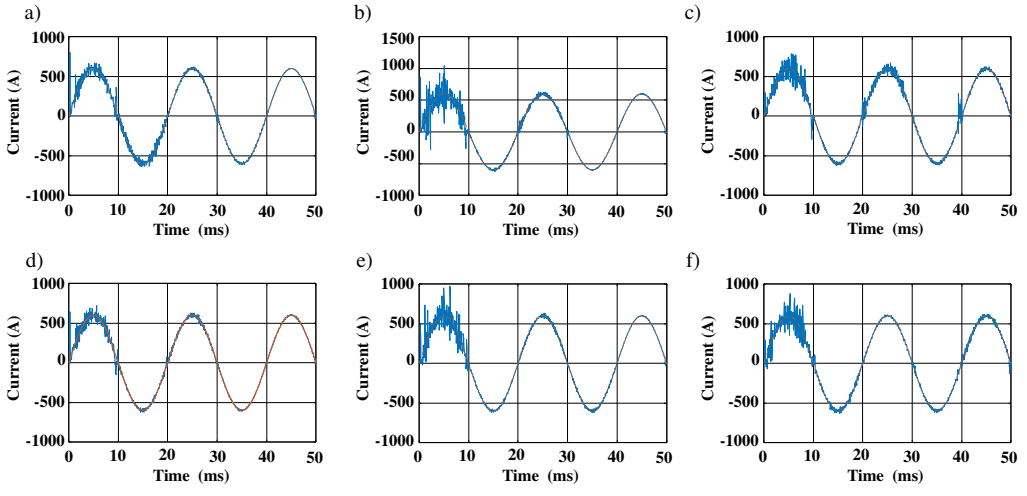

Fig. 11. The current filtered by the RLS-based interference-rejection algorithm with gauss white noise of different strength a) 5% in parallel; b) 10% in parallel; c) 15% in parallel; d) 5% in triangle; e) 10% in triangle; f) 15% in triangle.

5. Conclusions

In this paper, an adaptive filtering-based current reconstruction method with a magnetic sensor array is proposed to measure current in the three-phase current system. First, factors including the learning rate, forgetting factor, number of sensors, sensor position and conductor displacement

were analysed by numerical simulations. For 600 A current at 50 Hz, when the forgetting factor is 0.01, the amplitude relative error obtained with the RLS-based algorithm is $6 \times 10^{-4}\%$. Compared with the array containing two or three sensors, the four-sensor structure has better performance. From the simulations of sensor positions results that the RLS-based interference-rejection algorithm is more stable. The error variance in relation to the sensor position which changes from 15 mm to 25 mm is 130% in the parallel and 250% in the regular triangle structure. When a conductor displacement is within 6 mm, the error of the RLS-based algorithm is smaller compared with that of the LMS-based algorithm. The laboratory experiments were then carried out to demonstrate the effectiveness of the RLS-based algorithm. The results prove that the RLS-based algorithm can measure the target current in the three-phase alternating current system with the minimum error of 1%. In addition, the RLS-based algorithm is capable to filter gauss white noise. The standard deviation of the difference between the filtered signal and the real current signal is 11 A in the parallel and 24 A in the triangular structure. Nevertheless, the filtered result is not smooth in the first period. Further research is needed to improve this.

Acknowledgements

This project is supported by Sichuan Youth Science and Technology Innovation Team Fund under Grant 2017TD0009.

References

[1] Amin, S.M., Wollenberg, B. F. (2005). Toward a smart grid: power delivery for the 21st century. *IEEE Power & Energy Magazine*, 3(5), 34–41.

[2] Fang, X., Misra, S., Xue, G., Yang, D. (2012). Smart Grid – The New and Improved Power Grid: A Survey. *IEEE Communications Surveys & Tutorials*, 14(4), 944–980.

[3] Farhangi, H. (2009). The path of the smart grid. *IEEE Power & Energy Magazine*, 8(1), 18–28.

[4] Chan, J.Y.C., Tse, N.C.F., Lai, L.L. (2013). A Coreless Electric Current Sensor With Circular Conductor Positioning Calibration. *IEEE Transactions on Instrumentation and Measurement*, 62(11), 2922–2928.

[5] Suzuki, Y., Yamasawa, K., Hirayabayashi, A. (2008). Analysis of a Zero-Flux Type Current Sensor Using a Hall Element. *IEEE Translation Journal on Magnetics in Japan*, 9(1), 165–170.

[6] Khawaja, A.H., Huang, Q., Chen, Y. (2019). A Novel Method for Wide Range Electric Current Measurement in Gas-Insulated Switchgears With Shielded Magnetic Measurements. *IEEE Transactions on Instrumentation and Measurement*, 1–11.

[7] Freitas, P.P., Ferreira, R., Cardoso, S., Cardoso, F. (2007). Magnetoresistive sensors. *IEEE Translation Journal on Magnetics in Japan*, 19(16), 165221–165221.

[8] Popovic, R.S., Drljaca, P.M., Schott, C. (2002). Bridging the gap between AMR, GMR, and Hall magnetic sensors. *International Conference on Microelectronics*.

[9] Chen, K.-L., Chen, N. (2011). A New Method for Power Current Measurement Using a Coreless Hall Effect Current Transformer. *IEEE Transactions on Instrumentation and Measurement*, 60(1), 158–169.

[10] Weiss, R., Makuch, R., Itzke, A., Weigel, R. (2017). Crosstalk in Circular Arrays of Magnetic Sensors for Current Measurement. *IEEE Transactions on Industrial Electronics*, 64(6), 4903–4909.

[11] Rienzo, L.D., Bazzocchi, R., Manara, A. (2001). Circular arrays of magnetic sensors for current measurement. *IEEE Transactions on Instrumentation & Measurement*, 50(5), 1093–1096.

[12] Li, X., You, J., Shu, X., Kang, R. (2009). Electric current measurement using AMR sensor array. *International Conference on Mechatronics and Automation*. Changchun

[13] Bernieri, A., Ferrigno, L., Laracca, M., Rasile, A. (2017). An AMR-based Three Phase Current Sensor for Smart Grid Applications. *IEEE Sensors Journal*, 17(23), 7704–7712.

[14] Chen, Y., Huang, Q., Khawaja, A.H. (2019). An Interference-Rejection Strategy for Measurement of Small Current Under Strong Interference With Magnetic Sensor Array. *IEEE Sensors Journal*, 19(2), 692–700.

[15] Bazzocchi, R., Rienzo, L.D. (1999). Interference rejection algorithm for current measurement using magnetic sensor arrays. *Sensors & Actuators A Physical*, 85(1), 38–41.

[16] Itzke, A., Weiss, R., Weigel, R. (2019). Influence of the Conductor Position on a Circular Array of Hall Sensors for Current Measurement. *IEEE Transactions on Industrial Electronics*, 66(1), 580–585.

[17] Zhu, K., Lee, W.K., Pong, P.W.T. (2017). Non-Contact Capacitive-Coupling-Based and Magnetic-Field-Sensing-Assisted Technique for Monitoring Voltage of Overhead Power Transmission Lines. *IEEE Sensors Journal*, 17(4), 1069–1083.

[18] Diniz, P.S.R. (2013). Adaptive Filtering: Algorithms and Practical Implementation. *Bibtex Nuhag*.

[19] Giri, A.K., Arya, S.R., Maurya, R., Babu, B.C. (2018). Power Quality Improvement in Stand-alone SEIG based Distributed Generation System using Lorentzian Norm Adaptive Filter. *IEEE Transactions on Industry Applications*, (99), 1–1.

[20] Zanni, L., Boudec, J.Y.L., Cherkaoui, R., Paolone, M. (2017). A Prediction-Error Covariance Estimator for Adaptive Kalman Filtering in Step-Varying Processes: Application to Power-System State Estimation. *IEEE Transactions on Control Systems Technology*, 25(5), 1683–1697.

[21] Enayati, J., Moravej, Z. (2017). Real-time harmonics estimation in power systems using a novel hybrid algorithm. *IET Generation Transmission & Distribution*, 11(14), 3532–3538.

[22] Zhao, J., Wang, Z., Wang, J. (2016). Robust Time-Varying Load Modeling for Conservation Voltage Reduction Assessment. *IEEE Transactions on Smart Grid*, (99), 1–1.

[23] Zhou, N., Pierre, J.W., Trudnowski, D.J., Guttromson, R.T. (2007). Robust RLS Methods for Online Estimation of Power System Electromechanical Modes. *IEEE Transactions on Power Systems*, 22(3), 1240–1249.

[24] Jing, W., Geng, Y.S., Wang, J.H., Song, Z.X. (2005). Electric Current Measurement Using Magnetic Sensor Array Based on Kalman Filtering. *Automation of Electric Power Systems*.

[25] So, H.C. (2001). LMS-based algorithm for unbiased FIR filtering with noisy measurements. *Electronics Letters*, 37(23), 1418–1420.

[26] Feitosa, A.E., Nascimento, V. H., Lopes, C. G. (2018). Adaptive Detection in Distributed Networks using Maximum Likelihood Detector. *IEEE Signal Processing Letters*, (99), 1–1.

[27] Ali, H.S. (2008). *Kalman Filtering and RLS*. Hoboken, NJ USA: Wiley-IEEE Press.

[28] Ali, H.S. (2008). *RLS Algorithm*. Hoboken, NJ USA: Wiley-IEEE Press.

[29] Ali, H.S. (2008). *Performance of RLS and Other Filters*. Hoboken, NJ USA: Wiley-IEEE Press.

[30] Haykin, S.S. (2009). *Neural networks and learning machines*. Beijing, China: China Machine Press.

[31] TMR2104. (2019). *http://www.dowaytech.com/en/1800.html*